Genuine-multipartite-entanglement trends in gapless-to-gapped transitions of quantum spin systems

Anindya Biswas, R. Prabhu, Aditi Sen(De), and Ujjwal Sen

Harish-Chandra Research Institute, Chhatnag Road, Jhunsi, Allahabad 211 019, India

We investigate the behavior of genuine multiparticle entanglement, as quantified by the generalized geometric measure, in gapless-to-gapped quantum transitions of one- and two-dimensional quantum spin models. The investigations are performed in the exactly solvable one-dimensional XY models, as well as two-dimensional frustrated J_1–J_2 models, including the Shastry-Sutherland model. The generalized geometric measure shows nonmonotonic features near such transitions in the frustrated quantum systems. We also compare the features of the generalized geometric measure near the quantum critical points with the same for measures of bipartite quantum correlations. The multipartite quantum correlation measure turns out to be a better indicator of quantum critical points than the bipartite measures, especially for two-dimensional models.

I. INTRODUCTION

Recent developments at the interface of quantum information science and many-body physics indicate that quantum correlations, in particular, quantum entanglement [1], can potentially be a universal physical characteristic to investigate many-body phenomena. For example, entanglement has been proposed as a detector of quantum phase transitions (QPTs) in spin systems [2–4] and as a tool to develop and simplify efficient numerical simulations such as density matrix renormalization group [5]. Of late, the developments involving the numerical simulations using matrix product states [6], projected entangled pair states [7], and tensor network states [8] have established a strong connection between entanglement and many-body theory. At the same time, the behavior of entanglement has been investigated in many-body systems such as cold atomic gases in optical lattices [9] and trapped gaseous Bose-Einstein condensates [10]. On the other hand, information-theoretic quantum correlation measures such as quantum discord [11] have also been used to study critical phenomena in many-body systems [12]. In this paper, we focus our attention on multisite entanglement of many-body physical systems, integrable and nonintegrable.

The characterization of entanglement in physical systems is mostly restricted to bipartite entanglement due to the general unavailability of computable measures in the multipartite scenario. However, in some cases, it turns out that the bipartite-entanglement measures cannot capture the cooperative phenomena in the system [13,14], and therefore it is natural to look out for multipartite-entanglement measures to investigate such many-body systems [15].

Multipartite-entanglement measures, e.g., the geometric measure [16] (cf. [17]), global entanglement [18], and some other measures [19], have been used to describe many-body phenomena [20]. However, in general, they are hard to compute and it is therefore not possible to use them for states of arbitrary many-body systems. Recently, a genuine-multiparticle-entanglement measure called the generalized geometric measure (GGM) [21] was introduced which can be easily computed for pure states in arbitrary dimensions and of an arbitrary number of particles. It has since been found to be useful to study the genuine multiparty entanglement

present in systems such as resonating valence bond states and states of disordered systems [22]. In this paper, we apply the GGM to study quantum spin models, including frustrated ones [23,24]. Frustration appears in a many-body system if it is not possible to simultaneously and independently minimize all of the interaction terms of the corresponding Hamiltonian [24]. The characterization of such systems is typically hard to achieve [24]. We consider the following four classes of quantum spin systems:

(1) the quantum one-dimensional (1D) transverse XY model [25],

(2) the 1D antiferromagnetic J_1–J_2 Heisenberg model [26–29],

(3) the antiferromagnetic J_1–J_2 model on a two-dimensional (2D) lattice [23], and

(4) the Shastry-Sutherland model [30].

The choice of the above models is due to their immense importance in understanding the different exotic phases in many-body systems, including high-T_c superconductivity [31]. Moreover, the recent experimental realizations of such spin models in the laboratories [3,32–34], for example, in optical lattices [3,35], trapped ions [36], photons [37], and nuclear magnetic resonance [38], have led to the interesting possibility of the observation of the many-body effects described here in the laboratories. Towards the unfolding of such many-body effects, we apply the multiparty-entanglement measure, i.e., the GGM, to study the phase diagrams in these models from a multipartite-entanglement perspective. It is observed that the phase diagrams, so obtained, indicate transitions from gapless to gapped phases, and vice versa, in these models.

The approach chosen in the paper is as follows. Entanglement properties have been suspected to be related to a large variety of cooperative phenomena in many-body physics. However, the analysis of this suspicion is made difficult by the intractability of most entanglement measures, especially in the multiparty domain. The generalized geometric measure (GGM) is a recently proposed genuine-multiparty-entanglement measure and is, to our knowledge, the only measure that can be computed for any pure quantum state of an arbitrary number of parties in any dimension. We wish to use this fact to our advantage towards analyzing multiparty

entanglement in many-body systems. The proposal is to use the GGM as an order parameter to detect quantum phase transitions. We first use the GGM to check whether it can effectively capture the well-known quantum phase transition in the transverse *XY* model. It is to be noted that the quantum transverse *XY* model can be solved exactly, and it will therefore be satisfying to find that the GGM detects the quantum phase transition in this model precisely, without any concern for finite-size effects. Having obtained this result, we then look for the possibility of the GGM acting as a detector of quantum phase transitions in the other models, which are not exactly solvable and moreover in which the quantum phase transitions are not precisely known, by considering the other order parameters used in the literature. For comparison, we evaluate the bipartite quantum correlation measures towards detecting the quantum critical points of all the above models. We find that the GGM is a better indicator of quantum phase transitions than the bipartite measures, especially for two-dimensional lattice models.

The paper is organized as follows: In Sec. II, we present a formal definition of the genuine-multiparty-entanglement measure, viz., the GGM, and we show that the same can be expressed in terms of easily computable Schmidt coefficients. We also discuss the reasons for choosing GGM over bipartite measures such as concurrence and logarithmic negativity for the present investigations. Further results are presented in Sec. III where, in each section, we consider one of the quantum spin models. Sections III A, III B, III C, and III D deal, respectively, with the anisotropic *XY*, the 1D frustrated J_1–J_2 model, the 2D frustrated J_1–J_2 model, and the Shastry-Sutherland model. In Sec. IV, we compare the GGM with other bipartite quantum measures of shared quantum systems in terms of detecting QPTs. Finally, we draw our conclusions in Sec. V.

II. GENERALIZED GEOMETRIC MEASURE

In this section, we present a brief description of the GGM and show that it is efficiently computable for pure quantum states of an arbitrary number of parties. A pure quantum state $|\psi\rangle_{A_1,A_2,...,A_N}$, shared between N parties, $A_1, A_2, \ldots, A_N$, is said to be genuinely N-party entangled if it is not a product across any bipartite partition. The GGM of a pure quantum state $|\psi\rangle_{A_1,A_2,...,A_N}$ is defined as

$$\mathcal{E}\big(|\psi\rangle_{A_1,A_2,...,A_N}\big) = 1 - \Lambda_{\max}^2\big(|\psi\rangle_{A_1,A_2,...,A_N}\big). \qquad (1)$$

Here, $\Lambda_{\max}(|\psi\rangle_{A_1,A_2,...,A_N}) = \max |\langle\phi|\psi\rangle_{A_1,A_2,...,A_N}|$, where the maximization is taken over all pure states $|\phi\rangle$ which are not genuinely N-party entangled.

Let us enumerate some of the properties of GGM.

(1) $\mathcal{E}$ is nonvanishing for all genuine-multiparty-entangled states, and vanishing for others.

(2) $\mathcal{E}$ is monotonically nonincreasing under local (quantum) operations and classical communication. (The proof follows from the theorem stated below and Ref. [39].)

We now prove a theorem, where we show how the GGM can be expressed in terms of Schmidt coefficients.

Theorem. The generalized geometric measure (GGM) can be expressed as

$$\mathcal{E}(|\psi\rangle)$$
$$= 1 - \max\big\{\lambda_{\mathcal{A}:\mathcal{B}}^2 | \mathcal{A} \cup \mathcal{B} = \{A_1, \ldots, A_N\}, \mathcal{A} \cap \mathcal{B} = \emptyset\big\}, \qquad (2)$$

where $\lambda_{\mathcal{A}:\mathcal{B}}$ is the maximal Schmidt coefficient of $|\psi\rangle_{A_1,A_2,...,A_N}$ in the $\mathcal{A} : \mathcal{B}$ bipartite split.

Proof. The maximization involved in the definition of GGM, given in Eq. (1), is over all N-party pure quantum states $|\phi\rangle_{A_1,A_2,...,A_N}$ that are not genuinely multiparty entangled. The square of $\Lambda_{\max}(|\psi\rangle_{A_1,A_2,...,A_N})$ can be interpreted as the Born probability of an outcome in some quantum measurement on the multiparty quantum state $|\psi\rangle_{A_1,A_2,...,A_N}$. Since entangled quantum measurements are, in general, better than the product ones for any set of the subsystems involved, the maximization needs to be carried out only in a partition of $A_1, A_2, \ldots, A_N$ into two parts. In other words, the maximization in $\max |\langle\phi|\psi_{A_1,A_2,...,A_N}\rangle|$ is performed over the $|\phi\rangle_{A_1,A_2,...,A_N}$ that are the product across some bipartition, say, $\mathcal{A} : \mathcal{B}$. This is exactly the maximal Schmidt coefficient, $\lambda_{\mathcal{A}:\mathcal{B}}$, of the state $|\psi\rangle_{A_1,A_2,...,A_N}$ in the $\mathcal{A} : \mathcal{B}$ bipartite split. Note that $\lambda_{\mathcal{A}:\mathcal{B}}$ are increasing under local operations and classical communication (LOCC) [39]. This immediately implies that GGM ($\mathcal{E}$) is nonincreasing under LOCC. And, $\Lambda_{\max}(|\psi\rangle_{A_1,A_2,...,A_N})$ is the maximum of all such maximal Schmidt coefficients in all possible bipartite splits of the N parties. Hence, the theorem. ∎

The theorem makes it possible to calculate the GGM for any pure state of an arbitrary number of parties in arbitrary dimensions. This is due to the fact that the definition of GGM, given in Eq. (1), reduces to the calculation of squares of the maximal Schmidt coefficients across all bipartitions, as given in Eq. (2). So, for example, for calculating the GGM of a four-party symmetric state $|\psi\rangle_{ABCD}$, we have to consider $|\psi\rangle$ in the A:BCD and AB:CD partitions, and find the maximal Schmidt coefficients in these partitions. The GGM of $|\psi\rangle_{ABCD}$ is then $1 - \lambda^2$, where λ is the highest of these maximal Schmidt coefficients.

There are a large number of concepts that can be used to quantify entanglement. The reasons that we use the GGM here are as follows. It is widely believed that entanglement of many-body systems has an important bearing on the cooperative physical phenomena in those systems. Since a large number of particles (subsystems) is necessary for generating such effects, it is plausible that it is the multiparty entanglement that would better reveal the positions and characteristics of these cooperative phenomena. This belief is reinforced by the recent results demonstrating that bipartite-entanglement measures such as concurrence and logarithmic negativity cannot reliably capture the position of quantum phase transitions in some systems [13,14]. It is therefore all the more natural to look out for multipartite-entanglement measures to investigate such cooperative phenomena in many-body systems. The generalized geometric measure is, to our knowledge, the only measure of genuine multiparty entanglement that can be computed for any pure quantum state of an arbitrary number of parties in any dimensions. This led us to use it to study transitions in important many-body systems.

The scaling of the von Neumann entropy is a way to understand the multiparty-entanglement properties of quantum many-body states. In this case, the corresponding state $|\psi_N\rangle$ of, say, N spin-$\frac{1}{2}$ particles, is first divided into two parts, one of which consists of L particles while the other consists of the rest. Then the von Neumann entropy S_L of the subsystem of L particles corresponds to the entanglement of $|\psi_N\rangle$ in the $L : N - L$ bipartition. Note here that the entropy has to be found by using all the Schmidt coefficients of the density matrix of the subsystem.

In a path-breaking series of papers, a change in the scaling law, i.e., the behavior of S_L versus L, has been proposed to be an order parameter to detect quantum phase transitions [4,40]. The scaling of local von Neumann entropy, however, has important drawbacks. First, local von Neumann entropy is not a measure of entanglement for mixed quantum shared states. Second, and perhaps more important, is the fact that while scanning over a system parameter to "pin down" a phase transition, it is difficult, practically, to detect a change in the scaling law, especially for systems where finite-size calculations are essential, due to analytical intractability. This is because at every point in parameter space, we obtain a function. Scanning over the parameter space, we get a family of functions. Detecting phase transitions by looking for changes in the functional form is a mathematically difficult problem, especially if the functional forms are all approximate to begin with.

Both of these drawbacks are overcome by considering the GGM. The GGM is well defined for both pure and mixed states. Moreover, scanning over the parameter space, we obtain a surface defined on the parameter space because for every point of the parameter space, the GGM at that point is a real number. We then identify phase transitions with some drastic change in behavior of this surface.

Furthermore, to calculate the GGM, one should consider all possible bipartitions of the N-partite state [in the maximization given in Eq. (2)], which include bipartitions whose parts are not separately connected. On the other hand, in consideration of the scaling of von Neumann entropy, one usually considers connected clusters of lattice sites. However, there are important exceptions [41] where researchers have gone beyond this usual practice.

III. BEHAVIOR OF GGM NEAR GAPLESS-TO-GAPPED QUANTUM TRANSITIONS

In this section, we consider a series of paradigmatic quantum spin systems. They are taken up one by one in the different sections. Each section begins with a brief description of the Hamiltonian corresponding to the quantum system under study. Subsequently, we study the behavior of the ground state of these models, and investigate the advantage of considering the genuine-multipartite-entanglement measure in these models.

A. Anisotropic XY model

The Hamiltonian for the one-dimensional anisotropic quantum XY model of N quantum spin-half particles, arranged in an 1D array, is given by [25]

$$H_{XY} = \frac{J}{2}\left(\sum_{i=1}^{N}(1+\gamma)\sigma_i^x\sigma_{i+1}^x + (1-\gamma)\sigma_i^y\sigma_{i+1}^y\right) + h\sum_{i=1}^{N}\sigma_i^z, \tag{3}$$

where J, which has the units of energy, is of the same order as the coupling constant for the nearest-neighbor interaction, $\gamma \in (0,1]$ is the (dimensionless) anisotropy parameter, σ's are the Pauli spin matrices, and h, which again has the units of energy, represents the external transverse magnetic field applied across the system. In all of the models considered in this paper, we impose the periodic boundary condition. The quantum XY Hamiltonian can be diagonalized by applying Jordan-Wigner, Fourier, and Bogoliubov transformations [25]. At zero temperature, it undergoes a quantum phase transition driven by the transverse magnetic field at $\lambda \equiv h/J = 1$. Moreover, it is also known that the model is gapped for all field strengths except at the point where the quantum phase transition occurs. Such transitions have been detected by using bipartite-entanglement measures such as concurrence and multipartite-entanglement measures such as geometric measure [20,42]. We investigate the behavior of the genuine-multipartite-entanglement measure, viz., the GGM, of the ground state when it crosses from one gapped phase to another, through the gapless point.

The ground state of the system represented by the quantum XY Hamiltonian, as given in Eq. (3), can be analytically obtained by using Majorana fermions and it is also possible to get the eigenvalues of the local density matrices corresponding to the ground state, in different bipartitions [4,25]. The local density matrix corresponding to L consecutive sites can be obtained by calculating their correlators and magnetizations. The largest eigenvalue of the local density matrix corresponding to L sites, where $1 \leqslant L \leqslant N/2$, when subtracted from 1, gives the GGM. We have assumed here that the density matrices corresponding to nonconsecutive sites do not produce significant eigenvalues to contribute to the GGM. We have checked that this assumption remains valid for moderate-sized finite XY chains. The assumption is intuitively satisfactory as we are dealing with a nearest-neighbor interaction model. In Fig. 1, we have plotted the GGM and the derivative of the GGM for the ground state of the XY model with respect to the driving parameter, λ, for different values of the anisotropic constant γ. The divergence of the derivative of GGM captures the presence of the quantum phase transition at $\lambda = 1$. When $\gamma = 1$, which corresponds to the Ising model, the genuine multipartite entanglement is maximum when compared to the systems with lower values of γ.

B. 1D frustrated J_1–J_2 model

We will now consider the frustrated one-dimensional J_1–J_2 Heisenberg model, in which the nearest-neighbor couplings J_1 and the next-nearest-neighbor couplings J_2 are both antiferromagnetic. It was found that solid-state systems such as $SrCuO_2$ can be described by this model [43]. Moreover, advances in the field of cold atomic systems promise to create
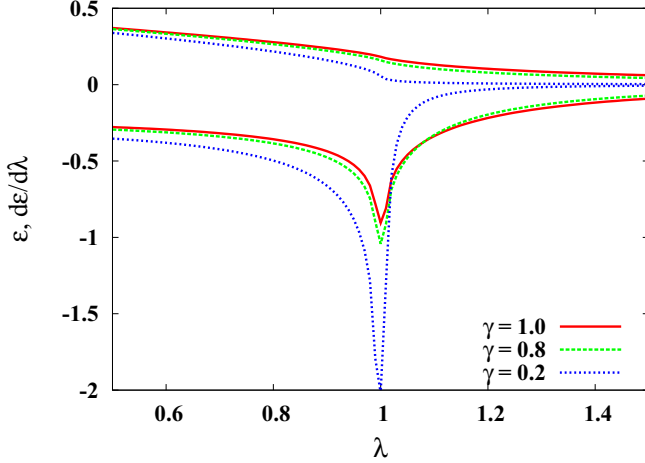
FIG. 1. (Color online) GGM of the transverse *XY* model. The GGM and its derivative (both dimensionless) are plotted on the vertical axis for the anisotropic transverse *XY* model for different anisotropy parameters γ, against the dimensionless system parameter λ on the horizontal axis. The plots are for the Ising ($\gamma = 1$), $\gamma = 0.8$, and $\gamma = 0.2$ models. The derivatives of the GGM diverge at the quantum critical point $\lambda = 1$. The cluster of three upper curves are for the GGM, while the lower ones are for their derivatives. For the purpose of the figure, we have used the eigenvalues corresponding to the single, two-, and three-site density matrices of the ground state.

and control such models in the laboratory [3]. The Hamiltonian of this model, with N lattice sites on a chain, can be written as

$$H_{1D} = J_1 \sum_{i=1}^{N} \vec{\sigma}_i \cdot \vec{\sigma}_{i+1} + J_2 \sum_{i=1}^{N} \vec{\sigma}_i \cdot \vec{\sigma}_{i+2}, \quad (4)$$

where J_1 and J_2 are both positive. In the parameter space, $\alpha \equiv J_2/J_1 = 0.5$ is known as the Majumdar-Ghosh point, and the system is highly frustrated there. For an even number of sites, the ground state at the Majumdar-Ghosh point is doubly degenerate, and the ground-state manifold is spanned by the two dimers $|\psi_{MG}^{\pm}\rangle = \Pi_{i=1}^{N/2}(|0\rangle_{2i}|1\rangle_{2i\pm1} - |1\rangle_{2i}|0\rangle_{2i\pm1})$. Note that the model is gapped at this point [26]. For $\alpha = 0$, the Hamiltonian reduces to the spin-$\frac{1}{2}$ Heisenberg antiferromagnet and, hence, the ground state, which is a spin fluid state having gapless excitations [44], can be studied by Bethe ansatz [45]. At other points, the ground state and the energy gap of this model were considered by using exact diagonalization, the density matrix renormalization group method, bosonization technique, etc. [29]. It is known that at $\alpha \approx 0.2411$, a phase transition from fluid to dimerization occurs [46]. In the weakly frustrated regime, $0 < \alpha \lesssim 0.24$, the system is gapless, and therefore critical [26,27]. The system enters a dimerized regime, and is gapped, for higher values of the coupling parameter.

We perform exact diagonalization of the Hamiltonian using TITPACK (version 2) developed by Nishimori [47] to find the ground state and then compute the GGM. In Fig. 2, the GGM is almost constant with respect to the driving parameter in the region when the system is gapless. It begins to increase with respect to the driving parameter near the phase transition point. However, due to the small system size that is accessible
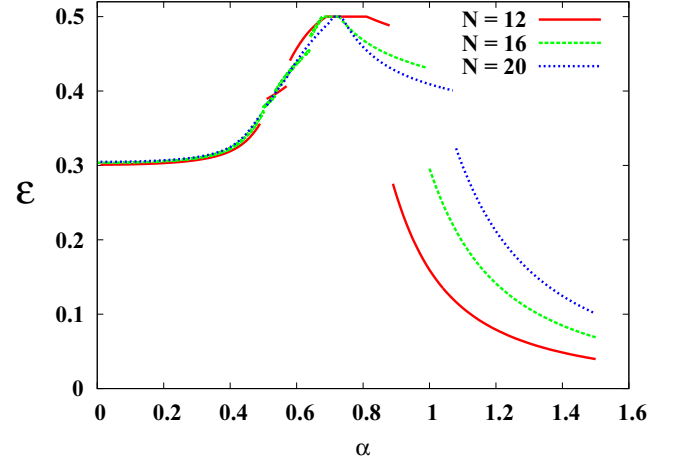

FIG. 2. (Color online) GGM for the 1D frustrated J_1–J_2 model. The GGM (dimensionless) is plotted on the vertical axis and system parameter α (dimensionless) is plotted along the horizontal axis. Note that the GGM starts to increase from its almost constant value of $\sim$0.3 in the gapless region, around $\alpha \approx 0.3$. We take a closer look at the figure in Sec. IV.

to study, it is difficult to locate the exact QPT point from the figure. Our investigation nevertheless reveals the behavior of multisite entanglement in the relevant parameter space of the finite-size 1D frustrated J_1–J_2 model.

The discontinuities in the GGM curves are arguably due to the finite and small system sizes. Note that the amounts of the discontinuities in Fig. 2 decrease with increase in the system size from $N = 12$ to $N = 20$ and it is plausible that they will disappear for larger systems. These discontinuities appear at avoided level crossings of the two lowest eigenvalues of the system Hamiltonian. Note that the behavior of entanglement entropy is also similar for this model (see Fig. 7 of Ref. [28]). Also, note that the GGM curves asymptotically go to zero for very high values of the driving parameter α, as then the spin chain decouples into two spin chains with nearest-neighbor interaction couplings, J_2.

C. 2D frustrated J_1–J_2 model

We now consider an arrangement of quantum spin-$\frac{1}{2}$ particles on a 2D square lattice, where nearest-neighbor spins (both vertical and horizontal) on the lattice are coupled by Heisenberg interactions, with coupling strengths J_1, and where all diagonal spins are coupled by the same interactions, with coupling strengths J_2. Both J_1 and J_2 are considered to be positive. The model has attracted a lot of attention [48] due to its connection with high-T_c superconductors and its similarity with magnetic materials such as Li_2VOSiO_4 and Li_2VOGeO_4 [49]. Although the different phases of the ground state of this model have been predicted by different numerical as well as approximate analytical methods [50], some debate remains. The Hamiltonian of the system is given by

$$H_{2D} = J_1 \sum_{\langle NN \rangle} \vec{\sigma}_i \cdot \vec{\sigma}_j + J_2 \sum_{\langle diagonals \rangle} \vec{\sigma}_i \cdot \vec{\sigma}_j, \quad (5)$$
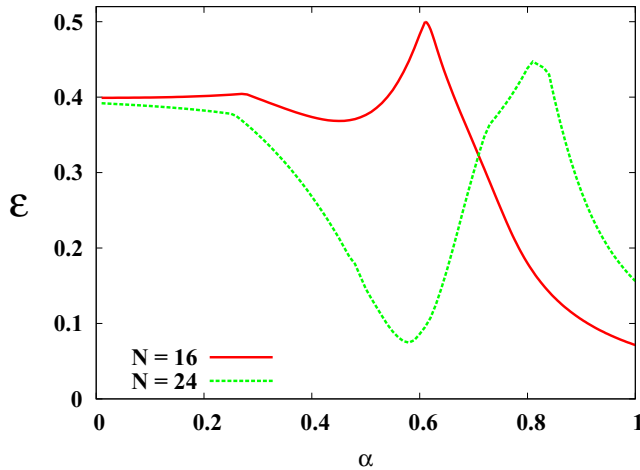
where J_1 and J_2 are antiferromagnetic.

FIG. 3. (Color online) GGM for the 2D frustrated J_1–J_2 model. The GGM (vertical) is plotted against the system parameter α (horizontal). Both of the quantities are dimensionless.

FIG. 4. The Shastry-Sutherland lattice. The solid lines represent the nearest-neighbor interactions with coupling strength J_1 between the lattice sites and the ones joined by the dashed lines represent next-nearest-neighbor interactions with coupling strength J_2.

In the classical limit, only a first-order phase transition from Néel to collinear at $\alpha \equiv J_2/J_1 = 0.5$ is exhibited by this model. The nature of the phase diagram changes when quantum fluctuations are present and, in this case, the exact phase boundaries are not known. Based on exact diagonalization, series-expansion methods, field-theory methods [50], etc., one expects that there are two long-range ordered (LRO) ground-state phases in the system, which are separated by quantum paramagnetic phases without LRO. These investigations predict that the first transition from Néel to dimer occurs at $\alpha = \alpha_1^c \in (0.3, 0.45)$, while the dimer to collinear transition happens at $\alpha = \alpha_2^c \in (0.6, 0.7)$. There are proposals to detect these phases in the laboratory and they demand a precise quantification of the low-temperature phase diagram of this model.

We investigate the behavior of genuine multipartite entanglement of the ground state and study its effectiveness to detect the transitions present in the system. To obtain the ground states, we use the exact diagonalization technique, as mentioned in the preceding section. In Fig. 3, we plot the GGM as a function of the driving parameter α. The nonanalyticity of the GGM with respect to the driving parameter α indicates that a Néel (gapless) to dimer (gapped) transition occurs at $\alpha \approx 0.27$ for $N = 16$ and $\alpha \approx 0.25$ for $N = 24$, while the dimer to collinear transition point is in the range $\alpha \in (0.61, 0.62)$ for $N = 16$ and $\alpha \approx 0.81$ for $N = 24$. In the case of the second transition, the $N = 24$ case predicts a transition at a point that is somewhat away from previous predictions. We believe that this is due to the fact that 24 is not a perfect square. The results indicate that the second transition is more sensitive to the lattice structure for such small systems. Just like in the 1D case, the GGM curves asymptotically go to zero for high α. This is because the spin lattice decouples into two spin lattices with nearest-neighbor interaction couplings, J_2, for very high values of the driving parameter α.

D. The Shastry-Sutherland model

In this section, we study the entanglement properties of systems where the interaction between particles can be modeled
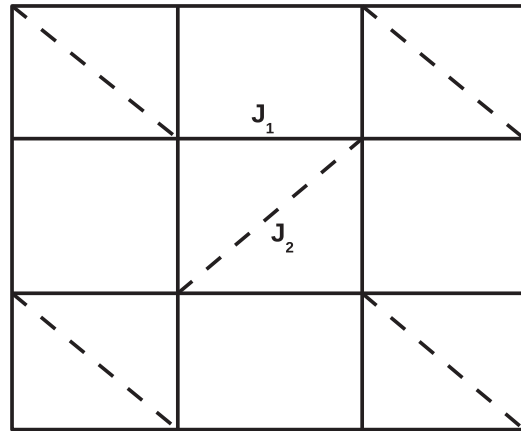
by the Shastry-Sutherland Hamiltonian [30]. In the insulators such as Sr Cu$_2$(BO$_3$)$_2$, the low-energy spin excitations reside on the spin-half copper ions which lie in two-dimensional layers decoupled from each other. The antiferromagnetic exchange couplings between the Cu ions are identical to the Shastry-Sutherland Hamiltonian. The lattice with schematic interactions, for this model, is given in Fig. 4 and the Hamiltonian is given by

$$H_{\text{SS}} = J_1 \sum_{NN} \vec{\sigma}_i \cdot \vec{\sigma}_j + J_2 \sum_{NNN} \vec{\sigma}_i \cdot \vec{\sigma}_j. \qquad (6)$$

Here, J_1 (>0) corresponds to the nearest-neighbor interaction (indicated by solid lines in Fig. 4) and J_2 (> 0) corresponds to the specific next-nearest neighbors (indicated by broken lines in Fig. 4). It is known that a simple product of singlet pairs, on the diagonal links, is the ground state of H_{SS} for sufficiently large $\alpha \equiv J_2/J_1$. It has been previously reported [51,52] that the system undergoes two quantum phase transitions driven by the quantum fluctuations: one is from Néel to an intermediate phase and the other one is from that intermediate phase to dimer. The nature of the intermediate phase is not yet clearly understood [53].

In Fig. 5, we plot the GGM as a function of α for 16 particles on a square lattice interacting via the Shastry-Sutherland Hamiltonian. There are clear signatures of these phase transitions in the figure at $\alpha \approx 1.05$ and for $\alpha \approx 1.53$, as have been predicted by other methods [51,52]. For very high J_2, the system consists of isolated dimers and the multisite entanglement vanishes. In Fig. 5, we find that the GGM becomes zero at $\alpha \geqslant 1.53$. The GGM curve is nonanalytic at the phase transition points in this model as well. Due to the computational constraints, we are able to report our finding only for $N = 16$. More specifically, we expect that studying the Shastry-Sutherland model requires an exact square structure with even numbers of spins on each side, and hence the next relevant lattice size is $N = 36$.
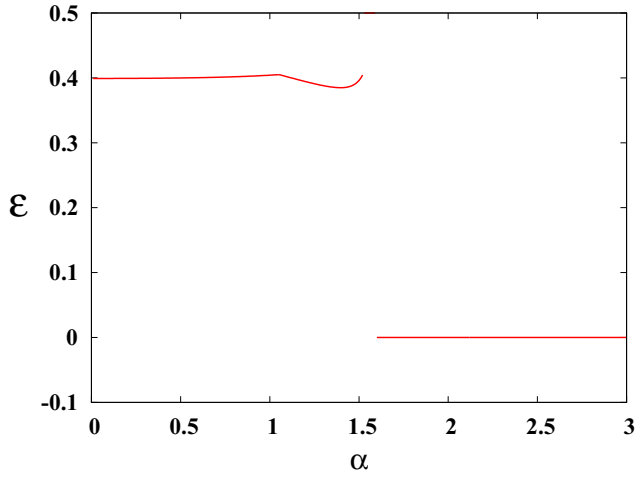
FIG. 5. (Color online) GGM for the Shastry-Sutherland antiferromagnet. GGM (on vertical axis) is plotted with respect to the system parameter α (on horizontal axis) for 16 spins. Both of the quantities are dimensionless.

IV. COMPARISON OF GGM WITH BIPARTITE QUANTUM MEASURES

Let us now compare the efficiency to detect the critical points by the genuine-multipartite-entanglement measure, GGM, with those by bipartite quantum characteristics in shared states of quantum spin models. We focus on the $N = 16$ case in all of the nonintegrable models considered in this paper. We calculate the concurrence [54], logarithmic negativity [55], quantum discord [11], and the shared purity [56] for the nearest-neighbor density matrices in these models.

The bipartite quantum correlation measures can be broadly classified into two classes: (i) the entanglement-separability paradigm and (ii) the information-theoretic paradigm. The concurrence and logarithmic negativity are measures of bipartite entanglement belonging to the entanglement-separability paradigm of quantum correlation measures, while quantum discord, which quantifies bipartite quantum correlation, belongs to the information-theoretic paradigm. The shared purity is a quantum characteristic of shared multipartite quantum systems which is different from quantum correlations. We briefly discuss the measures below.

Concurrence. For any two-qubit state, ρ_{AB}, the concurrence [54] is given by $\mathcal{C}(\rho_{AB}) = \max\{0, \lambda_1 - \lambda_2 - \lambda_3 - \lambda_4\}$, where the λ_i's are the square roots of the eigenvalues of $\rho_{AB}\tilde{\rho}_{AB}$ in decreasing order and $\tilde{\rho}_{AB} = (\sigma_y \otimes \sigma_y)\rho_{AB}^*(\sigma_y \otimes \sigma_y)$, with σ_y being the Pauli spin matrix.

Logarithmic negativity. The negativity of a bipartite quantum state ρ_{AB}, denoted by $\mathcal{N}(\rho_{AB})$, is defined as the sum of the negative eigenvalues of $\rho_{AB}^{T_A(T_B)}$, where $\rho_{AB}^{T_A(T_B)}$ denotes the partial transpose of ρ_{AB} with respect to $A(B)$. Then the logarithmic negativity [55] of ρ_{AB} is defined as

$$E_{\mathcal{N}}(\rho_{AB}) = \log_2[2\mathcal{N}(\rho_{AB}) + 1]. \tag{7}$$

The positivity of logarithmic negativity guarantees that the state is entangled.

Quantum discord. Quantum discord [11] for a bipartite state ρ_{AB} is defined as the difference between the total correlation

and the classical correlation of the state. The total correlation, defined as the quantum mutual information of ρ_{AB}, is given by

$$\mathcal{I}(\rho_{AB}) = S(\rho_A) + S(\rho_B) - S(\rho_{AB}), \tag{8}$$

where $S(\sigma) = -\mathrm{tr}(\sigma \log_2 \sigma)$ is the von Neumann entropy of the quantum state σ. The classical correlation, based on the conditional entropy, is defined as

$$\overleftarrow{\mathcal{J}}(\rho_{AB}) = S(\rho_A) - S(\rho_{A|B}). \tag{9}$$

Here,

$$S(\rho_{A|B}) = \min_{\{B_i\}} \sum_i p_i S(\rho_{A|i}) \tag{10}$$

is the conditional entropy of ρ_{AB}, conditioned on a measurement performed by B with rank-one projection-valued operators $\{B_i\}$, producing the states $\rho_{A|i} = \frac{1}{p_i}\mathrm{tr}_B[(\mathbb{I}_A \otimes B_i)\rho(\mathbb{I}_A \otimes B_i)]$, with probability $p_i = \mathrm{tr}_{AB}[(\mathbb{I}_A \otimes B_i)\rho(\mathbb{I}_A \otimes B_i)]$. $\mathbb{I}$ is the identity operator on the Hilbert space of A. Hence the discord can be calculated as [11]

$$\overleftarrow{\mathcal{D}}(\rho_{AB}) = \mathcal{I}(\rho_{AB}) - \overleftarrow{\mathcal{J}}(\rho_{AB}). \tag{11}$$

Here, the superscript "$\leftarrow$" on $\mathcal{J}(\rho_{AB})$ and $\mathcal{D}(\rho_{AB})$ indicates that the measurement is performed on the subsystem B of the state ρ_{AB}. Similarly, if measurement is performed on the subsystem A of the state ρ_{AB}, one can define a quantum discord as

$$\overrightarrow{\mathcal{D}}(\rho_{AB}) = \mathcal{I}(\rho_{AB}) - \overrightarrow{\mathcal{J}}(\rho_{AB}). \tag{12}$$

In our case, $\overleftarrow{\mathcal{D}}(\rho_{AB}) = \overrightarrow{\mathcal{D}}(\rho_{AB})$, which is a consequence of the periodic boundary condition used for our analysis.

Shared purity. Shared purity [56] is the difference between the "global" and "local" fidelities of an arbitrary (pure or mixed) state ρ. The global fidelity is a measure of the minimum distance of the state ρ from a globally pure state, while the local fidelity is a measure of the minimum distance of ρ from a locally pure state. The "global fidelity" of an N-party arbitrary (pure or mixed) quantum state, $\rho_{1,...,N}$, on $\mathcal{H} = \mathbb{C}^{d_1} \otimes \cdots \otimes \mathbb{C}^{d_N}$, is defined as

$$F_G = \max_{\{|\phi\rangle_{1,...,N} \in \mathcal{H}\}} {}_{1,...,N}\langle\phi|\rho_{1,...,N}|\phi\rangle_{1,...,N}, \tag{13}$$

where the maximization is performed over all elements (pure states) of $\mathcal{H}$. And the "local fidelity" of the same state is defined as

$$F_L = \max_{\{|\phi\rangle_{1,...,N} \in S\}} {}_{1,...,N}\langle\phi|\rho_{1,...,N}|\phi\rangle_{1,...,N}, \tag{14}$$

where the maximization is carried out over a certain set S of pure product states. For bipartite systems, the set S consists of all pure product states. The shared purity denoted by S_P is defined as

$$S_P = F_G - F_L. \tag{15}$$

Comparison. In Fig. 6, we compare the concurrence, logarithmic negativity, quantum discord, and shared purity with the GGM, calculated for the ground state of the 1D J_1–J_2 Hamiltonian consisting of 16 spins, with respect to the driving parameter α. The GGM is calculated for the 16-spin ground state, while the other quantities are calculated for the nearest-neighbor two-spin reduced density matrix of the same
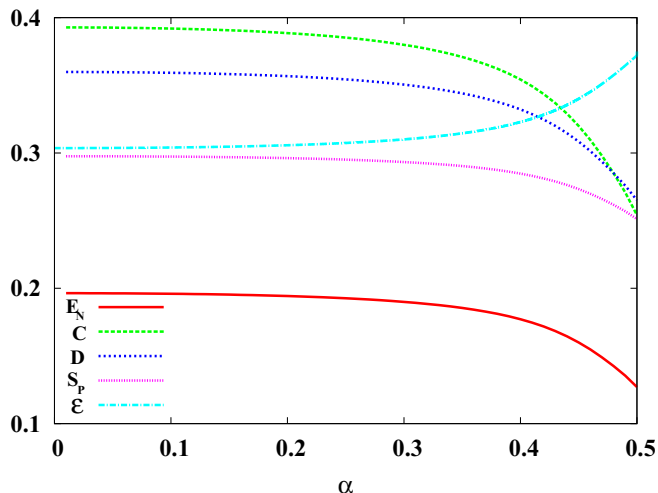
FIG. 6. (Color online) Logarithmic negativity, concurrence, quantum discord, shared purity, and GGM, with respect to the driving parameter α, for the 1D J_1-J_2 Hamiltonian consisting of 16 spins. Note that all quantities begin to deviate from their $\alpha = 0$ values above $\alpha \gtrsim 0.25$. The horizontal axis is dimensionless. For the vertical axis, logarithmic negativity and concurrence are measured in ebits, quantum discord in bits, while shared purity and GGM are dimensionless. We have denoted the quantum discord as D here, underlining the symmetric nature of the two-spin state.

FIG. 7. (Color online) Logarithmic negativity, concurrence, quantum discord, shared purity, and GGM, with respect to the driving parameter α, for the $N = 16$ 2D J_1-J_2 Hamiltonian. A magnified portion of the GGM curve signaling a QPT is plotted in the inset. The horizontal axis is dimensionless. All other dimensions and notations are as in Fig. 6.

16-spin state. The system remains in the gapless phase for $\alpha \lesssim 0.24$. It can be seen from the figure that all of the quantities begin to deviate from their $\alpha = 0$ values when $\alpha \gtrsim 0.25$. Note that the $\alpha = 0$ case corresponds to the isotropic Heisenberg nearest-neighbor antiferromagnetic chain. Although there is no definite signature of a QPT from any of the quantum measures, the critical point can be estimated to lie at $\alpha \approx 0.25$ by comparing with the $\alpha = 0$ case. Note that entanglement entropy was also used to estimate the quantum critical point by exact diagonalization in Ref. [28]. The quantity plotted there begins to deviate from its value at $\alpha = 0$ when $\alpha \gtrsim 0.25$. Here too, there is no clear signal at the QPT. However, the critical point was estimated to be at $\alpha \approx 0.25$. In Ref. [57], a multipartite-entanglement measure, the global entanglement, was used to study the 1D J_1-J_2 Hamiltonian. There was no clear signature of the QPT there either. It should be added, however, that the studies, despite not pinning down the QPT in the 1D J_1-J_2 model, do serve the important purpose of studying quantum correlation properties around this elusive QPT.

In Fig. 7, we plot the concurrence, logarithmic negativity, quantum discord, and shared purity, along with GGM, calculated for the ground state of the 16-spin 2D J_1-J_2 Hamiltonian, with respect to the driving parameter α. Again we compare the GGM with the bipartite measures. The GGM clearly signals both of the QPTs present in this model by virtue of the discontinuity of the derivative of the GGM with respect to α at the quantum critical points. The bipartite entanglement measures, viz., concurrence and logarithmic negativity, signal the second QPT at around $\alpha \approx 0.58$, where these quantities vanish. Quantum discord and shared purity also signal the second critical point at $\alpha \approx 0.6$, where the derivatives of
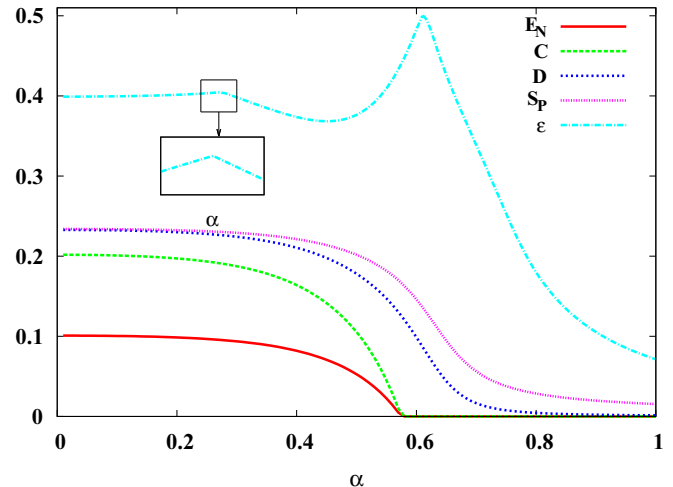
these quantities with respect to α are minimum. The bipartite measures do not conclusively detect the first quantum critical point. However, all of these bipartite measures begin to deviate from their values at $\alpha = 0$, when $\alpha \gtrsim 0.3$. It is clear that the multiparty measure is more efficient in this case than the bipartite measures in identifying quantum critical points.

In Fig. 8, we again plot the same bipartite measures and compare with the GGM, calculated for the ground state of the 16-spin Shastry-Sutherland Hamiltonian, with respect to the driving parameter α. The derivative of the GGM is discontinuous at both the quantum critical points, while the bipartite measures can only signal the second quantum critical
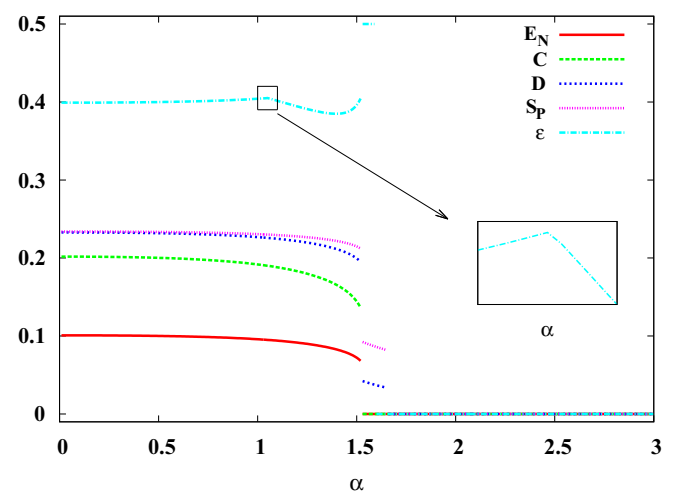

FIG. 8. (Color online) Logarithmic negativity, concurrence, quantum discord, shared purity, and GGM, with respect to the driving parameter α, for the $N = 16$ Shastry-Sutherland Hamiltonian. A magnified portion of the GGM curve signaling a QPT is plotted in the inset. The horizontal axis is dimensionless. All other dimensions and notations are as in Fig. 6.

point at $\alpha \approx 1.5$, above which they vanish. There is only a slight indication of the first QPT at $\alpha \approx 1$ above which the bipartite measures begin to deviate from their values at $\alpha = 0$. We therefore again find that the multiparty-entanglement measure is a better detector of quantum phase transitions than the bipartite measures.

V. CONCLUSIONS

An important classification scheme for multipartite-entangled quantum states is according to their separability in different partitions. The complexity of such a classification makes it difficult to obtain a unique multiparty-entanglement measure, even for pure quantum states. A comparison with the situation for mixed bipartite states is relevant here. While the entanglement of pure bipartite states can be uniquely characterized by a single entanglement measure, a variety of different measures exist for mixed bipartite states. In the case of multiparty quantum states, one can analogously have "pure" and "nonpure" forms of entanglement, corresponding, respectively, to genuine multiparty entanglement and ones that are not genuine. In this sense, the generalized geometric measure, which is a measure of genuine multiparty entanglement, quantifies the pure form of multiparty entanglement that is present in a multiparty quantum state.

We employed this measure to predict phase diagrams in quantum many-body systems. We began by using the measure to detect the quantum-fluctuation-driven phase transition in an exactly solvable model, viz., the quantum XY model. We subsequently applied the generalized geometric measure to prototype frustrated quantum spin models, in the one-dimensional antiferromagnetic J_1–J_2 model, the two-dimensional antiferromagnetic J_1–J_2 model, and the Shastry-Sutherland model. The ground states and the corresponding phase diagrams, for the frustrated models, are not known exactly, although there have been several predictions by different methods. We use exact diagonalization techniques to investigate the multipartite entanglement of the ground states of the frustrated models. The GGM is nonanalytic or its derivative is divergent at the quantum phase transition points in all of the models except the one-dimensional J_1–J_2 model. For the one-dimensional J_1–J_2 model, the fluid-dimer transition there is accompanied by a steep increase in the GGM. We have compared and contrasted the GGM with a number of bipartite measures of quantum correlation. The GGM appears to have an advantage in detecting the quantum critical points, particularly in the 2D frustrated quantum many-body systems.

[1] R. Horodecki, P. Horodecki, M. Horodecki, and K. Horodecki, Rev. Mod. Phys. **81**, 865 (2009).

[2] S. Sachdev, *Quantum Phase Transitions* (Cambridge University Press, Cambridge, 2011).

[3] M. Lewenstein, A. Sanpera, V. Ahufinger, B. Damski, A. Sen(De), and U. Sen, Adv. Phys. **56**, 243 (2007).

[4] L. Amico, R. Fazio, A. Osterloh, and V. Vedral, Rev. Mod. Phys. **80**, 517 (2008).

[5] S. R. White, Phys. Rev. Lett. **69**, 2863 (1992); Phys. Rev. B **48**, 10345 (1993); G. Vidal, Phys. Rev. Lett. **91**, 147902 (2003); **93**, 040502 (2004); F. Verstraete, D. Porras, and J. I. Cirac, *ibid.* **93**, 227205 (2004); K. A. Hallberg, Adv. Phys. **55**, 477 (2006).

[6] A. Klümper, A. Schadschneider, and J. Zittartz, J. Phys. A **24**, L955 (1991); Z. Phys. B **87**, 281 (1992); D. Perez-Garcia, F. Verstraete, M. M. Wolf, and J. I. Cirac, Quantum Inf. Comput. **7**, 401 (2007).

[7] F. Verstraete and J. I. Cirac, Phys. Rev. A **70**, 060302(R) (2004).

[8] H. Niggemann, A. Klümper, and J. Zittartz, Z. Phys. B **104**, 103 (1997); F. Verstraete and J. I. Cirac, arXiv:cond-mat/0407066; M. Levin and C. P. Nave, Phys. Rev. Lett. **99**, 120601 (2007); H. C. Jiang, Z. Y. Weng, and T. Xiang, *ibid.* **101**, 090603 (2008); J. Jordan, R. Orús, G. Vidal, F. Verstraete, and J. I. Cirac, *ibid.* **101**, 250602 (2008); Z. C. Gu, M. Levin, and X. G. Wen, Phys. Rev. B **78**, 205116 (2008).

[9] S. Trotzky, Y.-A. Chen, U. Schnorrberger, P. Cheinet, and I. Bloch, Phys. Rev. Lett. **105**, 265303 (2010); M. Cramer, M. B. Plenio, and H. Wunderlich, *ibid.* **106**, 020401 (2011); P. J. Pemberton-Ross and A. Kay, *ibid.* **106**, 020503 (2011), and references therein.

[10] T. Zibold, E. Nicklas, C. Gross, and M. K. Oberthaler, Phys. Rev. Lett. **105**, 204101 (2010); C. Gabriel, A. Aiello, W. Zhong, T. G. Euser, N. Y. Joly, P. Banzer, M. Förtsch, D. Elser, U. L. Andersen, Ch. Marquardt, P. St. J. Russell, and G. Leuchs, *ibid.* **106**, 060502 (2011), and references therein.

[11] L. Henderson and V. Vedral, J. Phys. A **34**, 6899 (2001); H. Ollivier and W. H. Zurek, Phys. Rev. Lett. **88**, 017901 (2001).

[12] R. Dillenschneider, Phys. Rev. B **78**, 224413 (2008); A. Dutta, U. Divakaran, D. Sen, B. K. Chakrabarti, T. F. Rosenbaum, and G. Aeppli, arXiv:1012.0653; B. Tomasello, D. Rossini, A. Hamma, and L. Amico, Europhys. Lett. **96**, 27002 (2011); Int. J. Mod. Phys. B **26**, 1243002 (2012); J. Mazero, L. C. Céleri, R. M. Serra, and M. S. Sarandy, Phys. Lett. A **376**, 1540 (2012); S. Campbell, L. Mazzola, G. De Chiara, T. J. G. Apollaro, F. Plastina, Th. Busch, and M. Paternostro, New J. Phys. **15**, 043033 (2013), and references therein.

[13] M.-F. Yang, Phys. Rev. A. **71**, 030302 (2005).

[14] X.-F. Qian, T. Shi, Y. Li, Z. Song, and C.-P. Sun, Phys. Rev. A **72**, 012333 (2005).

[15] M. N. Bera, R. Prabhu, A. Sen(De), and U. Sen, arXiv:1209.1523.

[16] A. Shimony, Ann. NY Acad. Sci. **755**, 675 (1995); H. Barnum and N. Linden, J. Phys. A **34**, 6787 (2001); R. Orús, Phys. Rev. Lett. **100**, 130502 (2008); R. Orús, S. Dusuel, and J. Vidal, *ibid.* **101**, 025701 (2008); R. Orús, Phys. Rev. A **78**, 062332 (2008); Q.-Q. Shi, R. Orús, J. O. Fjærestad, and H.-Q. Zhou, New J. Phys. **12**, 025008 (2010); R. Orús and T.-C. Wei, Phys. Rev. B **82**, 155120 (2010).

[17] M. Blasone, F. Dell'Anno, S. DeSiena, and F. Illuminati, Phys. Rev. A **77**, 062304 (2008).

[18] D. A. Meyer and N. R. Wallach, J. Math. Phys. **43**, 4273 (2002).

[19] A. Osterloh and J. Siewert, Phys. Rev. A **72**, 012337 (2005); Int. J. Quant. Inf. **04**, 531 (2006); D. Ž. Đoković and A. Osterloh, J. Math. Phys. **50**, 033509 (2009).

[20] T.-C. Wei and P. M. Goldbart, Phys. Rev. A **68**, 042307 (2003); T.-C. Wei, D. Das, S. Mukhopadyay, S. Vishveshwara, and P. M. Goldbart, *ibid.* **71**, 060305(R) (2005); T. R. de Oliveira, G. Rigolin, M. C. de Oliveira, and E. Miranda, Phys. Rev. Lett. **97**, 170401 (2006); D. Buhr, M. E. Carrington, T. Fugleberg, R. Kobes, G. Kunstatter, D. McGillis, C. Pugh, and D. Ryckman, J. Phys. A: Math. Theor. **44**, 365305 (2011).

[21] A. Sen(De) and U. Sen, Phys. Rev. A **81**, 012308 (2010); arXiv:1002.1253.

[22] R. Prabhu, S. Pradhan, A. Sen(De), and U. Sen, Phys. Rev. A **84**, 042334 (2011); H. S. Dhar and A. Sen(De), J. Phys. A: Math. Theor. **44**, 465302 (2011); R. Prabhu, A. K. Pati, A. Sen(De), and U. Sen, Phys. Rev. A **86**, 052337 (2012); H. S. Dhar, A. Sen(De), and U. Sen, New J. Phys. **15**, 013043 (2013); M. N. Bera, R. Prabhu, A. Sen(De), and U. Sen, Phys. Rev. A **86**, 012319 (2012).

[23] G. Misguich and C. Lhuillier, in *Frustrated Spin Systems*, edited by H. T. Diep (World Scientific, Singapore, 2003); C. Lhuillier, arXiv:cond-mat/0502464; F. Alet, A. M. Walczak, and M. P. A. Fisher, Physica (Amsterdam) A **369**, 122 (2006).

[24] M. Rasolt and Z. Tesanović, Rev. Mod. Phys. **64**, 709 (1992); M. Sigrist and T. M. Rice, *ibid.* **67**, 503 (1995).

[25] E. Lieb, T. Schultz, and D. Mattis, Ann. Phys. **16**, 407 (1961); E. Barouch, B. M. McCoy, and M. Dresden, Phys. Rev. A **2**, 1075 (1970); E. Barouch and B. M. McCoy, *ibid.* **3**, 786 (1971); B. K. Chakrabarti, A. Dutta, and P. Sen, *Quantum Ising Phases and Transitions in Transverse Ising Models* (Springer, Heidelberg, 1996).

[26] C. K. Majumdar and D. K. Ghosh, J. Math. Phys. **10**, 1388 (1969); **10**, 1399 (1969).

[27] S. R. White and I. Affleck, Phys. Rev. B **54**, 9862 (1996); S.-J. Gu, H. Li, Y.-Q. Li, and H.-Q. Lin, Phys. Rev. A **70**, 052302 (2004).

[28] R. W. Chhajlany, P. Tomczak, A. Wójcik, and J. Richter, Phys. Rev. A **75**, 032340 (2007).

[29] H. J. Mikeska and A. K. Kolezhuk, in *Quantum Magnetism*, edited by U. Schollwöck, J. Richter, D. J. J. Farnell, and R. F. Bishop (Springer, Berlin, 2004).

[30] B. S. Shastry and B. Sutherland, Physica B+C (Amsterdam) **108**, 1069 (1981).

[31] P. W. Anderson, Science **235**, 1196 (1987).

[32] K. Kim, M.-S. Chang, S. Korenblit, R. Islam, E. E. Edwards, J. K. Freericks, G.-D. Lin, L.-M. Duan, and C. Monroe, Nature (London) **465**, 590 (2010).

[33] J. Struck, C. Olschlager, R. Le Targat, P. Soltan-Panahi, A. Eckardt, M. Lewenstein, P. Windpassinger, and K. Sengstock, Science **333**, 996 (2011); J. Simon, W. S. Bakr, R. Ma, M. E. Tai, P. M. Preiss, and M. Greiner, Nature (London) **472**, 307 (2011).

[34] J. Zhang, M.-H. Yung, R. Laflamme, A. Aspuru-Guzik, and J. Baugh, Nat. Commun. **3**, 880 (2012).

[35] I. Bloch, J. Dalibard, and W. Zwerger, Rev. Mod. Phys. **80**, 885 (2008); C. Nayak, S. H. Simon, A. Stern, M. Freedman, and S. Das Sarma, *ibid.* **80**, 1083 (2008).

[36] D. Leibfried, R. Blatt, C. Monroe, and D. Wineland, Rev. Mod. Phys. **75**, 281 (2003); H. Häffner, C. Roos, and R. Blatt, Phys. Rep. **469**, 155 (2008).

[37] X.-S. Ma, B. Dakic, W. Naylor, A. Zeilinger, and P. Walther, Nat. Phys. **7**, 399 (2011).

[38] X. Peng, J. Zhang, J. Du, and D. Suter, Phys. Rev. Lett. **103**, 140501 (2009); J. Zhang, T.-C. Wei, and R. Laflamme, *ibid.* **107**, 010501 (2011); K. R. K. Rao *et al.*, Phys. Rev. A **88**, 022312 (2013).

[39] M. A. Nielsen, Phys. Rev. Lett. **83**, 436 (1999); G. Vidal, *ibid.* **83**, 1046 (1999); J. Mod. Opt. **47**, 355 (2000).

[40] J. Eisert, M. Cramer, and M. B. Plenio, Rev. Mod. Phys. **82**, 277 (2010).

[41] J. P. Keating, F. Mezzadri, and M. Novaes, Phys. Rev. A **74**, 012311 (2006).

[42] A. Osterloh, L. Amico, G. Falci, and R. Fazio, Nature (London) **416**, 608 (2002); T. J. Osborne and M. A. Nielsen, Phys. Rev. A **66**, 032110 (2002).

[43] M. Matsuda and K. Katsumata, J. Magn. Magn. Mater. **140–144**, 1671 (1995).

[44] R. B. Griffiths, Phys. Rev. **133**, A768 (1964); C. N. Yang and C. P. Yang, *ibid.* **150**, 327 (1966).

[45] H. Bethe, Z. Phys. **71**, 205 (1931).

[46] F. D. M. Haldane, Phys. Rev. B **25**, 4925 (1982); K. Okamoto and K. Nomura, Phys. Lett. A **169**, 433 (1992).

[47] H. Nishimori, AIP Conf. Proc. **248**, 269 (1992).

[48] P. Chandra and B. Doucot, Phys. Rev. B **38**, 9335 (1988); E. Dagotto and A. Moreo, Phys. Rev. Lett. **63**, 2148 (1989); F. Figueirido, A. Karlhede, S. Kivelson, S. Sondhi, M. Rocek, and D. S. Rokhsar, Phys. Rev. B **41**, 4619 (1990); N. Read and S. Sachdev, Phys. Rev. Lett. **66**, 1773 (1991); H. J. Schulz and T. A. L. Ziman, Europhys. Lett. **18**, 355 (1992); R. Darradi, O. Derzhko, R. Zinke, J. Schulenburg, S. E. Krüger, and J. Richter, Phys. Rev. B **78**, 214415 (2008), and references therein.

[49] R. Melzi, P. Carretta, A. Lascialfari, M. Mambrini, M. Troyer, P. Millet, and F. Mila, Phys. Rev. Lett. **85**, 1318 (2000); H. Rosner, R. R. P. Singh, W. H. Zheng, J. Oitmaa, S. L. Drechsler, and W. E. Pickett, *ibid.* **88**, 186405 (2002); R. Nath, A. A. Tsirlin, H. Rosner, and C. Geibel, Phys. Rev. B **78**, 064422 (2008); T. Yildirim, Phys. Rev. Lett. **101**, 057010 (2008); Q. Si and E. Abrahams, *ibid.* **101**, 076401 (2008).

[50] J. Richter and J. Schulenberg, Eur. Phys. J. B **73**, 117 (2010); J. K. Kim and M. Troyer, Phys. Rev. Lett. **80**, 2705 (1998); T. Pardini and R. R. P. Singh, Phys. Rev. B **79**, 094413 (2009).

[51] C. H. Chung, J. B. Marston, and S. Sachdev, Phys. Rev. B **64**, 134407 (2001).

[52] M. Albrecht and F. Mila, Europhys. Lett. **34**, 145 (1996).

[53] W. Zheng, J. Oitmaa, and C. J. Hamer, Phys. Rev. B **65**, 014408 (2001); M. A. Hajj and J.-P. Malrieu, *ibid.* **72**, 094436 (2005); R. Darradi, J. Richter, and D. J. J. Farnell, *ibid.* **72**, 104425 (2005); S. Moukouri, *ibid.* **78**, 132405 (2008).

[54] W. K. Wootters, Phys. Rev. Lett. **80**, 2245 (1998).

[55] G. Vidal and R. F. Werner, Phys. Rev. A **65**, 032314 (2002).

[56] A. Biswas, A. Sen(De), and U. Sen, Phys. Rev. A **89**, 032331 (2014).

[57] R. Eryiğit, Int. J. Theor. Phys. **48**, 885 (2009).